# NUMERICAL STUDY OF THE EFFECTS OF ORBITAL DEBRIS SHAPE AND OBLIQUITY ON ITS PERFORATION ABILITY

**Patrick Domingo [(1)], Igor Telichev [(2)]**

*[(1)] Department of Mechanical Engineering, University of Manitoba, E2-327 EITC, 75A Chancellors Circle, Winnipeg, MB R3T 5V6, Canada; E-mail: domingop@myumanitoba.ca*
*[(2)] Department of Mechanical Engineering, University of Manitoba, E2-327 EITC, 75A Chancellors Circle, Winnipeg, MB R3T 5V6, Canada; E-mail: igor.telichev@umanitoba.ca*

## ABSTRACT

Analysis of fragments from the DebriSat test and the Satellite Orbital debris Characterization Impact Test (SOCIT) have shown that orbital debris is not expected to be spherical and, more closely, can be categorized by thin plates ("flakes") or rod-like shapes. The design equations for the Micrometeoroid and Orbital Debris (MMOD) shield, such as those created by NASA, are based on experiments involving spherical projectiles to represent the space debris. So, to continue using such design equations for the development of spacecraft protection against real-life debris, the link between the spherical projectiles and the threat-equivalent non-spherical projectiles should be established.

A numerical methodology was developed to quantitatively measure the ability of a projectile with a specific shape to perforate spacecraft shielding. The modelling approach employs the utilization of smoothed particles hydrodynamics method (SPH) and the finite element method (FEM) in the Lagrangian formulation to simulate the hypervelocity impact of differently shaped cylindrical projectiles on the shielding. The craters' depth in the impacted semi-infinite plate behind the shielding is used as a metric to characterize the threat from a cylindrical projectile of a particular shape. By comparing the craters' depth, the cylindrical projectiles can be considered equivalent to a smaller or larger sphere.

The performed study revealed that for aluminum projectiles impacting aluminum plates, plate-like and rod-like cylindrical projectiles could be equivalent to spheres of up to 72% more massive or larger in terms of ability to perforate the double plate shield. The method was demonstrated using projectiles of a mass equal to a 6 mm sphere in normal (0-degree) impact at 7km/s. The equivalent sphere predictions made from measuring semi-infinite plate crater size were verified by performing standard ballistic limit test simulations on Whipple shields using design equations created by NASA.

The developed methodology provides an expedited way to determine an arbitrarily shaped projectile's equivalent spherical projectile when designing MMOD shielding. Additionally, the developed methodology can be used to compare projectiles under different conditions such as different velocity, incidence angle, yaw angle, or material.

## 1 INTRODUCTION

### 1.1 Passive spacecraft protection

Passive protection in the form of shielding is implemented in order to protect spacecraft against collisions from small untrackable space debris. The purpose of the shielding is to serve as a sacrificial material to prevent the MMOD perforaton of the spacecraft in critical areas. The passive protection on spacecraft shielding is designed to stop a specific size of space debris and smaller. One of the earliest types of spacecraft shielding is the Whipple Shield (WS), which consists of two plates separated by a distance. The principle of operation for the WS is to break up the impacting debris projectile into a cloud of fine particles using the front bumper plate. The debris cloud then spreads over a larger surface area, reducing the potential threat onto the rear wall. With increasing projectile impact velocity (at the hypervelocity range), portions of the cloud can melt or vaporize. The fragmentation of the debris and distribution of the debris momentum over the larger area reduces the thickness and, therefore, the weight of the shielding required for protection. More sophisticated spacecraft shieldings that were developed after the WS, such as the Stuffed Whipple Shield (SWS) or Multi-Shock Shield (MSS), also operate on the same principles.

### 1.2 Projectile shape

The development and design of spacecraft shielding are based on the results of experimental hypervelocity impact (HVI) tests and corresponding numerical simulations. The HVI tests replicate the space debris impact conditions and gauge the specifications of the shielding necessary to prevent spacecraft perforation by a particular size projectile. The HVI tests are costly therefore there are practical limitations on the frequency and manner they are performed. One such limitation is the use of spherical projectiles to represent the space debris impacting the shielding. Spherical projectiles

provide uniformity between different experiments since accounting for other shapes is not practical due to the limited number of tests that can be performed.

Analysis of fragments in previous ground-based experiments such as the Satellite Orbital debris Characterization Impact Test (SOCIT) [1] and DebriSat [2] reveal that real space debris is not sphere-like. Instead, debris can more accurately be categorized as thin plates ("flakes") or rod-like shapes. Therefore, there is a discrepancy between the conditions of experiments used for shielding design and the real conditions in Earth's orbit. However, this discrepancy does not invalidate the existing literature data. Instead, there need only be a method to relate previous spherical data with non-spherical predictions.

There have been many previous attempts to study the effects of the projectile shape on shielding. The studies were performed experimentally, such as in [3] and, more recently, numerically such as in [4]. Of particular note are J. Hiermaier and F. Schafer's works in 2003 [5], wherein a modified ballistic limit equation (BLE) was thereby relating literature spherical data to be adjusted to account for ellipsoidal projectiles. However, these studies' main limitation is that the results are limited to or effective only for specific conditions. Furthermore, the methods employed by previous studies are not conducive to application for different impact parameters. A method to expedite the study of shape effects in HVI would help build a more comprehensive knowledge base.

### 1.3 Objective

To develop a methodology to determine the relative perforation abilities of differently shaped projectiles in hypervelocity impact on Whipple shields.

## 2 METHOD: SEMI-INFINITE CRATER

The traditional method to measure the performance of spacecraft shielding against a particular projectile is to perform ballistic limit tests. This method involves a trial and error approach to obtain pass-or-fail conclusions. Since the objective requires studying differently shaped projectiles, such a method demands an unreasonably large number of tests. While a numerical approach reduces cost requirements and provides versatility in adjusting input parameters, performing the many ballistic limit simulations still involves long-time investments.

The craters produced on semi-infinite targets from projectiles in HVI are well studied, where penetration equations provide an estimate of the crater depth produced by a particular projectile. Furthermore, some studies were performed to account for non-spherical shape effects [6]. Naturally, a projectile that penetrates deeper (produces a deeper crater) into a semi-infinite plate is more likely to perforate through a body with finite thickness. In dual or multi-plate shielding, the HVI fragmentation phenomenon introduces complexity in the sequential impact of the debris cloud on the rear wall. However, it is assumed that the many craters produced by the projectile's debris cloud onto a semi-infinite plate can still be used to gauge the projectile's ability to perforate through a finite body.

The semi-infinite plate crater (SPC) numerical model was developed to create relative comparisons between differently shaped projectiles in terms of their ability to perforate the WS (double plate shield). The model allows the input of a projectile of arbitrary size and shape then provides an output metric used as a basis for comparing different input projectiles. The output for the SPC model is the crater depth of the largest crater produced by the debris cloud, which is then assumed to represent the perforation ability of the original projectile. The use of crater depth as an intermediary metric reduces the number of trials required to make comparisons between different input parameters.

The SPC model was developed in commercial software Ansys Autodyn. All additional simulations were also developed and run through Autodyn. Due to the complexity of material behaviour in HVI, smoothed particle hydrodynamics (SPH) method was used to model most of the components. The finite element method was incorporated to model parts that did not involve large deformations.

## 3 SPC MODEL

### 3.1 Material Model

All bodies in the SPC model were modelled using the aluminum material definition obtained from [7]. The model was able to successfully predict the hole dimensions produced in the aluminum bumper in hypervelocity impact testing. The details of the material model are presented in Table 1. Values not listed have a value of zero.

Additional study of the material model was performed for the debris clouds generated by cylindrical projectiles. Experiments described in [8] that include cylinders at various orientations impacting a bumper at approximately 7 km/s were replicated in simulation. The experiments involved both Aluminum 6061-T6 and Aluminum 2024-T4 material. The material model for the latter was obtained from [9].

The debris clouds of the HVI generated by the material model were qualitatively compared with images of the debris cloud experimentally obtained in [8]. In addition, velocities of the debris cloud leading edge (tip velocity) were also compared. Qualitatively, there was good agreement between numerical and experimental results on the shape and features of the debris cloud. At a near-zero yaw angle, there is less than 5% error for the tip velocity in numerical results. However, with increasing

yaw angle, the tip velocity error increases to 10.7% at 25 degrees. In all cases, the numerical model overestimated the tip velocity. Therefore, the material model is effective in modelling zero yaw and normal impacts involving cylinders.

*Table 1. Aluminum 6061-T6 material model.*

| Mie-Gruneisen equation of state | |
|---|---|
| Gruneisen coefficient | 1.97 |
| C1, m/s | $5.24 * 10^3$ |
| S1 | 1.4 |
| Reference Temperature, K | 293 |
| Specific heat, J/kgK | 885 |
| Johnson-Cook strength model | |
| Shear modulus, kPa | $2.6 * 10^7$ |
| Yield strength, kPa | $3.24 * 10^5$ |
| Hardening constant, kPa | $1.14 * 10^5$ |
| Hardening exponent | 0.42 |
| Strain rate constant | 0.002 |
| Thermal softening exponent | 1.34 |
| Melting temperature, K | 925 |
| Reference strain rate, 1/s | 1 |
| Strain rate correction | 1st order |
| Johnson-Cook failure model | |
| D1 | −0.77 |
| D2 | 1.45 |
| D3 | −0.47 |
| D5 | 1.6 |
| Melting temperature, K | 925 |
| Reference strain rate, 1/s | 1 |

### 3.2 SPC Model Geometry

The SPC model is configured in a way similar to the Whipple shield, simply consisting of two plates. However, the rear wall is replaced by a semi-infinitely thick plate. Figure 1 and Figure 2 show an outline of the different parts of the model.

The projectile shown in Figure 1 and Figure 2 corresponds to a cylinder with a length-to-diameter ratio L/D=1. However, the model was also run for cylinders with a different L/D while maintaining a mass equivalent to a 6-mm sphere. All projectiles impact normal to the bumper at 7km/s. The bumper is 1.5 mm thick, corresponding to the minimum required for 6 mm spheres from literature design equations [10].

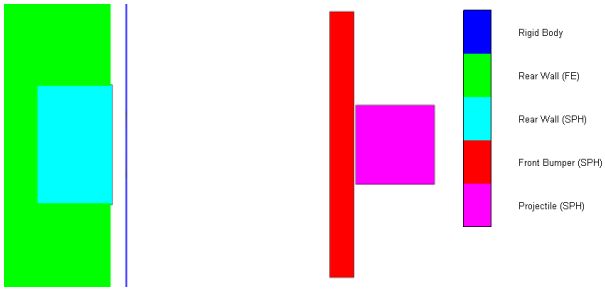


*Figure 1. Cross-section side-view of SPC model.*

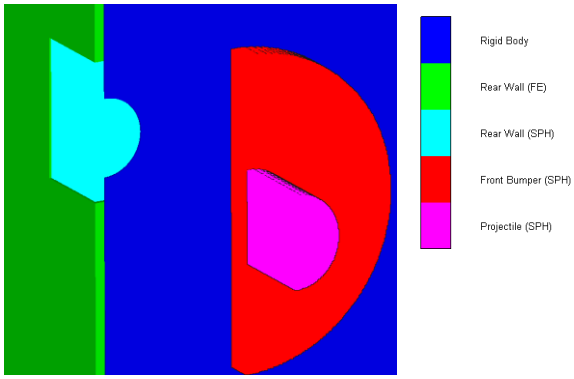


*Figure 2. Cross-section oblique-view of SPC model.*

Almost all the parts were modelled using the SPH method due to the fragmentation of the projectile and the large deformations at the crater of the rear wall. However, due to the high computational cost of using the SPH method, the geometries of the parts were reduced to the minimum required to maintain consistent results. The portion of the rear wall modelled using SPH was therefore kept only large enough to contain the central largest crater produced by the debris cloud.

To model the rest of the semi-infinite plate, finite elements (FE) were used. The FE were rigidly joined to the SPH nodes along the boundary of the SPH and FE in the rear wall. The two parts, therefore, behaved as a single body representing the rear wall. The geometric sizes of both the FE and SPH portions of the rear wall were chosen such that they were just large enough to have negligible influence on the crater produced by the debris cloud. The dimensions of the FE and SPH portions of the rear wall were determined in a trial and error process. The crater depth produced by a specific projectile was measured as the geometry of the rear wall was incrementally changed. The trial and error procedure was performed until consistency in the crater depth was reached. Note that this procedure was similar to the procedure used to determine various characteristics of the

SPH model, such as the mesh density of the FE or the minimum planar size of the front bumper.

The separation between the front bumper and the rear wall, referred to as the standoff distance $S$, was reduced to $S$ =15mm to further reduce computational time. This decision was made with the assumption that standoff distance would have a negligible effect on how SPC results can be applied. However, analysis of results, described later in section 4, showed that the standoff has a significant influence on the relative differences in perforation ability of differently shaped projectiles.

### 3.3 Rigid Body Blocker

Since the output desired from the model was the depth of the semi-infinite plate crater, it was assumed that only the largest crater was necessary to model. Therefore, only the largest crater produced by the debris cloud determined the pass or fail conclusion for the projectile onto spacecraft shielding. Furthermore, it was assumed that the peripheral fragments would have negligible influence on the central crater. This assumption is reasonable because the central portion of the debris cloud for normal impact contains fragments with the largest momentum.

A rigid body was placed between the front bumper and the rear wall to allow only passage and impact from the central portion of the debris cloud. The opening in the rigid body was centred along the velocity vector of the projectile. By introducing the rigid body blocker, the computational requirements of the model were reduced significantly.

The size of the rigid body opening was minimized such that the geometry of the other parts in the model could also be reduced further. Of particular importance was the reduction in the size of the SPH portion of the rear wall, which contained the majority of the SPH nodes. However, the opening in the rigid body still required to be large enough to contain the debris cloud fragments that had a significant influence on the main crater. Using a trial-and-error procedure, the crater produced by a specific projectile's debris cloud was measured as the opening size was increased. This procedure was repeated until consistency in crater depth was reached. For these trials, the crater was measured at a specific simulation time before the crater had fully formed. This was done because only the consistency of the crater depth value was required.

The ideal rigid body opening size was found to depend on the features of the debris cloud. Figure 3 shows an example of the variation in crater depth produced by an L/D=1 cylindrical projectile's debris cloud as the opening size was increased. In the case of cylindrical projectiles, the trials showed that the largest crater depth in the rear wall depended mainly on fragments contained in what is known as the front cone of the debris cloud. The front cone of the debris cloud produced by a L/D=1 cylinder is shown in Figure 4, which corresponds to the rigid body opening size indicated by the red arrow in Figure 3.

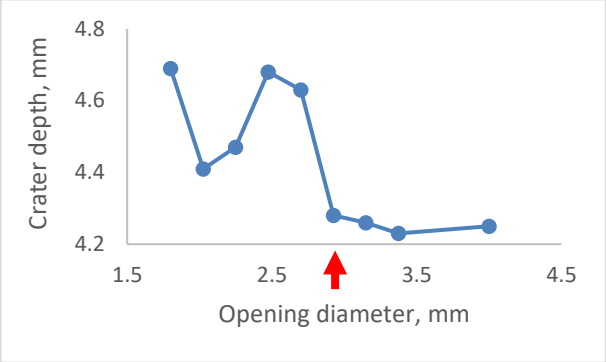


*Figure 3. Crater depth produced by L/D=1cylinder debris cloud vs rigid body opening.*

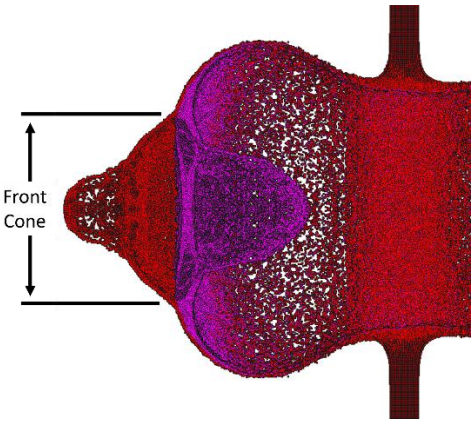


*Figure 4. Example debris cloud model of L/D=1 cylinder after impacting bumper at 7km/s.*

### 3.4 Verification procedure

Verification of the numerical model itself was done by determining the minimum required number of SPH nodes to receive converged numerical results. In addition, the error in energy was maintained at less than 5% of total energy. Convergence was achieved by reducing the variation of the desired output of the model (crater depth) to within 5% while increasing the total number of SPH nodes. This verification procedure is shown in Figure 5 for 6-mm spherical projectile. Similar conclusions were made for equal-mass cylindrical projectiles. The number of nodes corresponds to the amount in a quarter of the model, as the model has two planes of symmetry.

After the various crater depths of equal mass but differently shaped projectiles were obtained, it became possible to determine the equivalent sphere for each cylindrical projectile. Each cylindrical projectile was equivalent to a different-mass sphere in terms of the crater produced by their debris clouds. The crater depth was assumed to represent the perforation ability of the projectile in a Whipple shield configuration.

The equivalent sphere conclusions from the SPC results were checked with literature using standard ballistic limit tests in simulation. These tests involved specific cylindrical projectiles impacted against a Whipple shield designed for the cylinder projectile's equivalent sphere. All the cylinders were of equal mass to a 6-mm sphere; therefore, the cylinders were generally impacted against Whipple shields intended for spheres larger than 6 mm. The bumper and rear wall sizing were obtained from Whipple shield design equations [10].

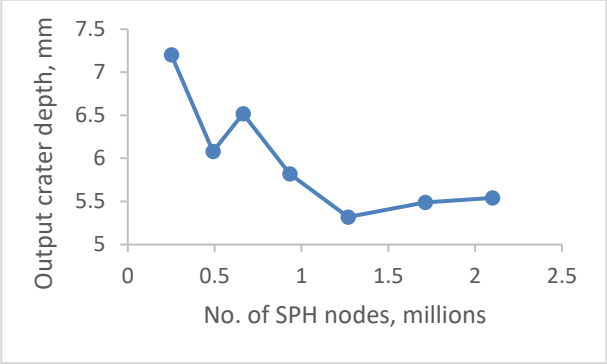


*Figure 5. Convergence of debris cloud crater depth in SPC model for 6-mm spherical projectile at 7km/s.*

The numerical ballistic limit verification tests were performed in a trial-and-error fashion. For each cylinder projectile, the "effective" sphere size corresponded to the Whipple shield thicknesses according to the literature design equations. The trial and error procedure involved the incremental increase or decrease in effective sphere size and the observation of perforation or spallation in the shielding's rear wall. For each cylinder shape, the procedure is performed until the Whipple shield is sufficiently thick such that impacting cylinder can no longer cause perforation or spallation in the rear wall. Ideally, the effective sphere size required to protect against each cylinder projectile would be equal to the cylinder's equivalent sphere result obtained from the SPC model.

The trial-and-error process of determining a specific projectile's effective sphere using the numerical ballistic limit tests is ultimately a method to determine the impacting cylinder's perforation ability on its own. However, this procedure requires many more trials and therefore more time to complete. In comparison, the SPC model uses crater depth as an intermediary metric to require only one trial for each specific shape.

## 4 RESULTS

### 4.1 Debris cloud

The shape and the tip velocity of the debris cloud are dependent on the shape of the projectile impacting the bumper. Examples of the debris clouds for cylinders such as the L/D=1/3 flake or L/D=5/3 rod impacting at 7 km/s are shown in Figure 6. The features of the debris clouds were qualitatively found to be in good agreement with experimental results for L/D=1 in [8] and for flake-like in [11]. Furthermore, the material model was partially validated for cylindrical projectiles, described in section 3.1.

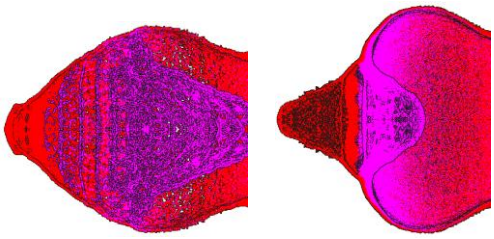

*Figure 6. Examples of debris cloud for flake L/D=1/3 (left) and L/D=5/3 (right) after impacting bumper at 7 km/s.*

Past a certain point in L/D, rod-like cylinder projectiles retained a portion of their original unfragmented body even after normal impact with the bumper at 7 km/s. An example of the unfragmented portion is shown in Figure 7 for L/D=3. In this situation, the unfragmented portion poses a significant risk to the rear wall. Additional tests revealed that increasing the thickness of the bumper reduced the size unfragmented portion. However, further study is still required to quantify the relationship between the bumper and high L/D rod-like cylinders. For consistency, the SPC model used a constant bumper thickness for all projectiles. Therefore, rod-like cylinders that produced unfragmented projectiles were excluded from the SPC model.

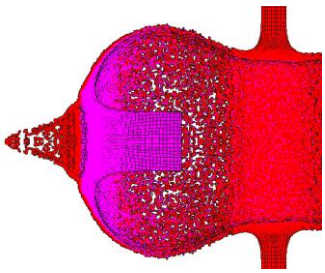

*Figure 7. Debris cloud and unfragmented portion produced by L/D=3 impacting bumper at 7km/s.*

### 4.2 Sphere equivalence

An example of how the crater depth is measured in the SPC model after impact from debris cloud is shown in Figure 8, which corresponds to crater formed by L/D=2/3 cylinder's debris cloud. The depth was measured from the original surface of the undeformed rear wall up to the deepest part of the crater. The crater was always centered along the axis of the cylinder projectile's velocity vector. SPC model's simulation time extended up to the point when the crater has stopped increasing in size.

The results for the cylinders and spheres input into the

SPC model are shown in Figure 9 and Figure 10, respectively. The cylinders are all of the equal mass to the 6-mm diameter sphere. All projectiles had an impact velocity of 7 km/s. All parts in the SPC model consisted of the Aluminum 6061-T6 material described previously in section 3.1. The SPC model was run for standoff distance $S$ =15mm.

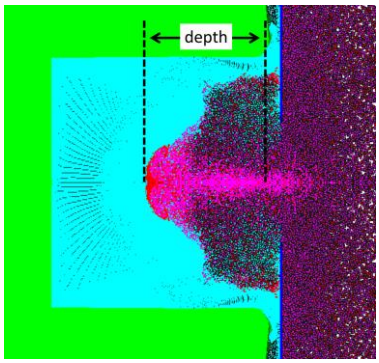


*Figure 8. Measurement of crater depth for L/D=2/3 cylinder's debris cloud.*

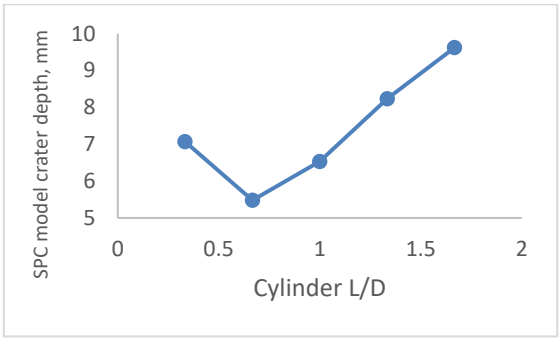


*Figure 9. SPC model results for input cylinders of mass equivalent to 6-mm sphere at S=15mm.*

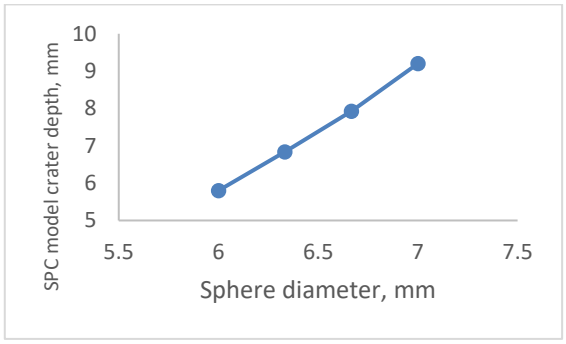


*Figure 10. SPC model results for input spheres of increasing size at S=15mm.*

The relationship between crater depth and sphere diameter was approximated as linear with an $R^2$ =0.99. The cylinder SPC results were input into the linear sphere relationship to obtain cylinder-sphere equivalence in terms of the crater depth in the SPC model. These results are shown in Figure 11. From the results, the effect of shape on a projectile of a particular mass is significant. The most extreme case among the shapes tested is the L/D=5/3 cylinder, which is equivalent to a 72% more massive sphere.

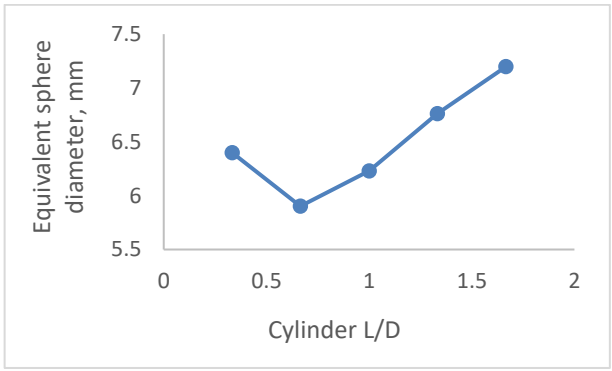


*Figure 11. Threat-equivalent sphere size for differently shaped cylinders of equal mass to 6mm sphere.*

The relationship between projectile shape and the potential severity of its damage onto the Whipple shield is incompletely defined. The work described in this paper features projectiles only in normal impact with zero yaw. In the case of dangerous shapes such as high L/D cylindrical rods, it is natural to assume that zero yaw impact represents the worst-case scenario. However, the uncertainty is yet undefined, requiring shielding designs to potentially have excessive or insufficient protection. Future work is still required to further study the perforation ability of different projectile shapes with non-normal impact and non-zero yaw angles. Future studies involving different impact parameters may be expedited with the development of the SPC model.

### 4.3 Comparison with literature

The Whipple shield design equations from [10] were used to verify the effectiveness of the equivalent-sphere results from the SPC. A trial-and-error procedure was performed where the cylinders described in section 4.2 were impacted against Whipple shields with iteratively increasing plate thicknesses until the ballistic limit was reached. The procedure was described in more detail previously in section 3.4. The numerical model used for the Whipple shield ballistic limit simulations was similar in design to the SPC model, containing a combination of SPH, FE and a rigid body blocker to reduce computational cost.

The Whipple shield ballistic limit simulations were performed for cylinder L/D=1/3 and L/D=5/3 at standoff $S$ =15mm. The simulations were similarly performed for the cylinders' equivalent sphere as a form of calibration between design equations and the numerical model. The calibration tests found that the numerical model overestimated the damage caused by the projectile debris cloud. Conversely, it was possible that the design equations were unsuited for such small standoff

distances. The calibration tests found that the Whipple shield at $S = 15$ mm required effective spheres 16% larger than expected. The 16% increase in effective sphere size represented the discrepancy between the numerical model used and the literature design equations.

After applying calibration, the cylinder ballistic limit trials showed that the equivalent spheres obtained from the SPC model were generally consistent with the expectations from the design equations. The effective sphere size for cylinders L/D=1/3 and L/D=5/3 were within 5% larger than the equivalent sphere obtained from the SPC model.

The ballistic limit simulations were also attempted at standoff distance $S = 100$mm. At this standoff distance, the design equations were able to protect against trial spherical projectiles without requiring calibration. However, the effective sphere sizes of cylinder L/D=1/3 and L/D=5/3 were found to be more than 30% larger than the expected equivalent sphere size obtained from SPC model at $S = 15$mm.

The verification trials showed that the equivalent sphere results from the SPC model are effective only for the specific standoff distance used. The results were otherwise inadequate for determining the effective spheres of cylinders at other standoff distances. It is hypothesized that debris clouds produced by differently shaped projectiles react differently to the spacing, with cylinder debris cloud having a reduced spread than spherical debris clouds. Cylindrical projectiles, therefore, pose a more significant threat to Whipple shields with increasing standoff spacing. Future work is required to quantify the relationship between cylinder-sphere equivalence and standoff spacing.

## 5 CONCLUSION

The conclusions of the work described in this paper are as follows:

1. The developed SPC model is effective at approximating the equivalent sphere for differently shaped cylinders in terms of the projectiles' ability to perforate Whipple shields impacting normal at 7 km/s.
2. Equivalence between projectiles of different shapes is dependent on the standoff distance for Whipple shields. Flake-like or rod-like projectiles are equivalent to increasingly more massive spheres as standoff increases during normal impact.
3. The developed method has potential application to determine threat equivalence between projectiles that differ in other parameters such as impact angle, yaw angle or velocity.

### Acknowledgments

This work was supported by the Natural Sciences and Engineering Research Council of Canada (Discovery Grant no. 402115-2012).

## 6 REFERENCES

[1] Williamsen, J., Schonberg, W. and Jenkin, A. (2011) On the effect of considering more realistic particle shape and mass parameters in MMOD risk assessments. *Advances in Space Research*, **47**, 1006-1019.

[2] Murray, J., et al. (2019) Analysis of the DebriSat fragments and comparison to the NASA standard satellite breakup model. In *Proc. 1st International Orbital Debris Conference*, Houston, Texas.

[3] Morrison, H. (1972) A preliminary investigation of projectile shape effects in hypervelocity impact of a double-sheet structure. *NASA TN D-6944*.

[4] Carrasquilla, M. and Miller, J. (2017) Shape effect analysis of aluminum projectile impact on whipple shields. In *Proc. 14th Hypervelocity Impact Symposium*, Canterbury, Kent, UK.

[5] Hiermaier, S., Schafer, F. and Schneider, E. (2003) Ballistic limit equations for the normal impact of unyawed ellipsoid-shaped projectiles on aluminum whipple shields. In *Proc. 54th International Aeronautical Congress*, Bremen, Germany.

[6] Schafer, F., et al. (2001) Shape effects in hypervelocity impact on semi-infinite mettalic targets. *International Journal of Impact Engineering*, **26**, 699-711.

[7] Corbett B. (2006) Numerical simulations of target hole diameters for hypervelocity impacts into elevated and room temperature bumpers. *International Journal of Impact Engineering*, **33**, 431-440.

[8] Piekutowski, A. (1987) Debris clouds generated by hypervelocity impact of cylindrical projectiles with thin aluminum plates. *International Journal of Impact Engineering*, **5**, 509-518.

[9] Kay, G. (2003) Failure modeling of Titanium 6Al-4V and Aluminum 2024-T3 with the Johnson-Cook Material Model. *DOT/FAA/AR-03/57*.

[10] Christiansen, E. (2009) Handbook for designing MMOD protection, *NASA, TM-214785*.

[11] Piekutowski, A. (1990) A simple dynamic model for the formation of debris clouds. *International Journal of Impact Engineering*, **10**, 453-471.